Coupled Thermal-Hydraulic/Electromagnetic Analysis and Interpretation of the Test Results of the ITER TFPRO2 OST1 Conductor

Roberto Zanino, Fabrizio Bellina, *Member, IEEE*, Pier Luigi Ribani, *Member, IEEE*, and Laura Savoldi Richard

***Abstract*—The THELMA code is used to study the coupled thermal-hydraulic electro-magnetic problem of the current and temperature distribution inside the TFPRO2 Nb_3Sn SULTAN sample, which was tested in 2007. The code computes self-consistent voltage and temperature values both on the jacket, where they are measured, and inside the cable, where they are more directly representative of the conductor performance. The measured temperature gradients, related to non-uniform Joule heating at the joint and in the high-field region, as well as to non uniform current distribution, are reasonably well reproduced by the model, together with the voltage-current characteristics.**

***Index Terms*—Fusion reactors, ITER, SULTAN samples, superconducting magnets.**

I. Introduction

THE performance of several different Nb3Sn cable-in-conduit conductors (CICC) for the International Thermonuclear Experimental Reactor (ITER) Toroidal Field (TF) coils is being tested in the SULTAN facility at Villigen PSI, Switzerland [1], using short conductor samples ∼3.5 m long; a part of these tests was specifically devoted to the EU samples TFPRO1 and TFPRO2 [2]. One of the test issues so far is how the current distribution in the cable may affect the results in a way peculiar to the SULTAN configuration rather than to the coil; in turn, this current distribution is increasingly related to the temperature distribution inside the cable, as the quench is approached. The THELMA code is best suited to study this coupled problem, as it combines an electromagnetic model of the cable [3], including a detailed description of the jacket [4], with a multi-solid multi-channel thermal-hydraulic model of the CICC [5]. THELMA was validated for several types of transients and superconducting materials in short samples [6]–[8]. In particular, the code computes self-consistent voltage and temperature values both on the jacket, where they are measured, and inside the cable, where they are more directly representative of the conductor performance. While the current distribution effects for the ITER TF reference conductor sample are parametrically studied with THELMA in a companion paper [9], and the left leg of TFPRO2 is studied in [10] from a purely electromagnetic point of view, here we concentrate on the right leg of TFPRO2, where a strand produced by Oxford Superconducting Technology (called OST1) was used [11]. The choice of this sample for our analysis is related to the fact among others that TFPRO2 was very well diagnosed, in terms of both temperature and voltage traces at different locations along and across the conductor. Our aim here is to assess the role of thermal-hydraulics on the interpretation of the conductor test via the self-consistent computation of temperature profiles along and across the conductor together with the voltage evolution, and the comparison with experimental results.

Manuscript received August 23, 2008. First published June 26, 2009; current version published July 15, 2009. This work was supported in part by the Italian Ministry for University and Research (MUR) and the participation of RZ and LSR to the TFPRO2 tests was supported by EURATOM mobility. LSR is also a grateful recipient of a Politecnico di Torino fellowship "Giovani ricercatori".

R. Zanino and L. Savoldi Richard are with the Dipartimento di Energetica, Politecnico, I-10129 Torino, Italy (e-mail: roberto.zanino@polito.it).

F. Bellina is with Università di Udine, Italy (e-mail: fabrizio.bellina@uniud.it).

P. L. Ribani is with Università di Bologna, Italy (e-mail: pierluigi.ribani@mail.ing.unibo.it).

Color versions of one or more of the figures in this paper are available online at http://ieeexplore.ieee.org.

Digital Object Identifier 10.1109/TASC.2009.2018205

II. Experimental Setup

TFPRO2 is a SULTAN sample with standard configuration. Two different short ITER TF conductor samples (legs) are connected at the bottom of a vertical layout through a joint (∼0.42 m long) and are electrically fed through terminations (∼0.35 m long) at the top. The dual-channel CICC has the central channel blocked from the joint inlet up to ∼1.5 m downstream.

Details about the conductor layout can be found in [1]. The electrical diagnostics include voltage taps and voltage rings (Sj, Sc), as shown in Fig. 1(a). The standard thermal-hydraulic diagnostics foreseen for the SULTAN tests [1], consisting mainly of a set of thermometers positioned on the jacket, were enhanced in the so-called TFPRO2 re-test as detailed in [12] and shown in Fig. 1(b). Of relevance here are the inlet helium temperature $T_{\rm in}$, the temperature T4 measured downstream of the joint and just (∼250 mm) upstream of the SULTAN magnetic field peak, the temperature T6 measured about one pitch length of the last cabling stage $(L_{\rm p})$ downstream from T4, and the temperature T8 measured $\sim 1/6\, L_{\rm p}$ further downstream. Each of these sensors "Tx" has a corresponding "Txa" sensor located at the same axial coordinate, but opposite azimuthal location.

Current sharing temperature $(T_{\rm CS})$ and critical current $(I_{\rm C})$ measurements were performed during the tests, to assess the conductor DC performance.

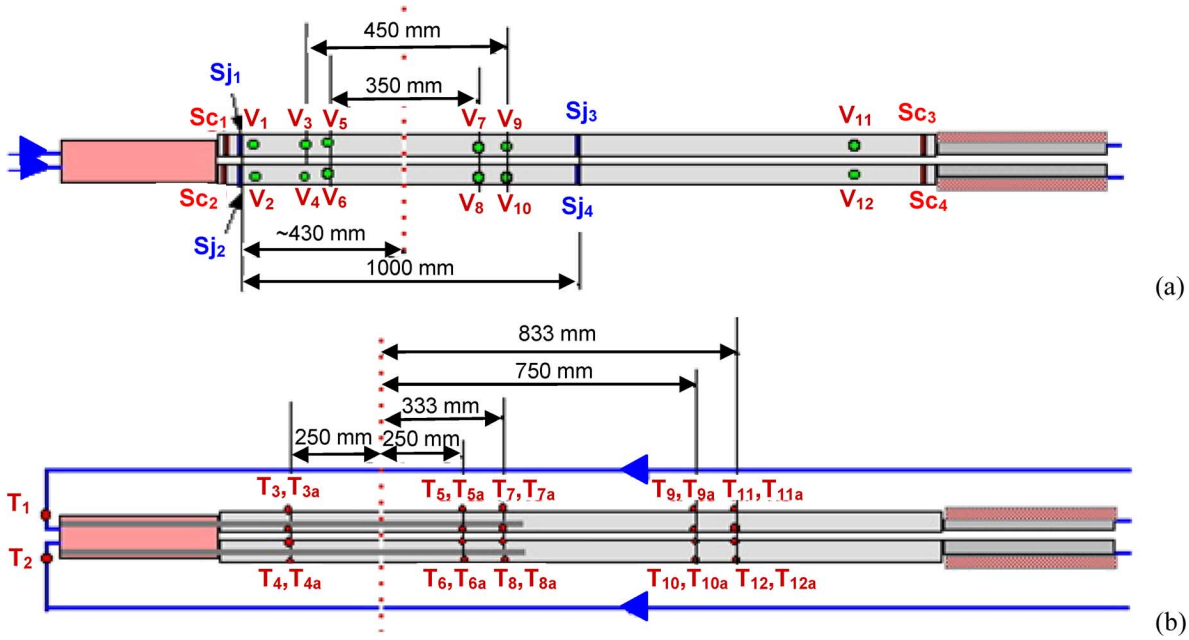

Fig. 1. SULTAN electrical (a) and thermal-hydraulic (b) diagnostics for the TFPRO2 re-test (courtesy of P. Bruzzone).

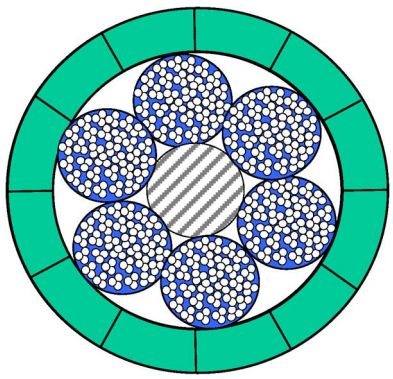

Fig. 2. THELMA discretization of the TFPRO2 cross-section.

III. Input and Assumptions

Simulations in this paper are performed considering the strands grouped in the 6 petals, which in the jargon of the model define 6 cable elements (CE), see Fig. 2. From the electromagnetic point of view, the jacket is discretized in 12 jacket elements [4]; from the thermal-hydraulic point of view, 6 hydraulic channels (one for each petal) + 1 Jacket, thermally coupled through the following heat transfer coefficients (all $\mathrm{W/m^2K}$), similar in value to those reported in [13]: 100, between He and CE; 50, between He and jacket; 50, between He in adjacent petals (advective heat transfer between them being neglected, for the sake of simplicity). Each of the CICC components has a different temperature in the model, which is a function of the coordinate along the CICC and of time.

The measured inlet temperature in the right leg $T_{\mathrm{in}}(t)$ (accounting for the difference between the measured inlet temperatures in the two legs of ~30 mK in the baseline run at 4.5 K [12]) and transport current $I(t)$ are used as boundary conditions. It should be noted that using this boundary condition for T_{in} in the simulation setup amounts to neglecting heat transfer between the two legs through the joint, and this is fully justified only if the inlet temperatures in the two legs are the same, which is not necessarily true to the high accuracy requested here. The analysis of a single leg therefore introduces some uncertainty in the computed temperatures downstream of the joint. For the run that we are considering here, the heat transfer can be estimated from the raw signals as leading to an additional increase of ~60 mK with respect to the temperatures computed by the model downstream of the joint. In the simulation, the pressure p_{in} is set at 10 bar, which is in the measured range, while p_{out} is set such as to reproduce the measured mass flow rate of about 2.5 g/s.

Only the cable is considered in detail in the electromagnetic model, while the joint and termination are represented by stars of resistors; the resistance of these resistors in parallel gives the correct (measured) value of joint and termination resistances and their spread corresponds to the non uniformity of the electric contact between each petal and joint/termination. With reference to the CE numbering in the Figures below, we use the following values (all $\mathrm{n\Omega}$) for the joint star: (4.65, 4.20, 4.77, 5.36, 5.64, 6.42), and for the termination star: (5.44, 6.50, 7.43, 8.24, 6.83, 5.38). Following the same strategy as in [10], these values have been chosen such as to find the best fit of the voltage signals at the voltage rings Sc, Sj, and at the voltage taps V4V10 (high field region), V1V2 (joint) and V12T (termination), see Fig. 1(a), as well as the calorimetric agreement between computed and measured temperatures at T4 and T4a (i.e., downstream of the joint), see below. Note that the corresponding half resistance on the right leg side amounts to 0.83 $\mathrm{n\Omega}$, to be compared with a measured total resistance of $\sim$ 1.3 $\mathrm{n\Omega}$, and that the star of resistances is a simplified (diagonalized) version of the full resistance matrix considered in [9] as a reasonable approximation of a detailed 3D model of the joint. Note also that, due to the wrapping of the petals, the coupling losses related to

inter-petal current loops, i.e. the only ones which can be modeled with the utilized 6 CE model, are much lower than those related to the intra-petal current loops (not modeled).

A cable exponent $n = 3.3$ was determined as best fitting the V-I characteristic across the high-field region (HFR) and $L_{\rm p} = 450\ {\rm mm}$ was used in the simulations. The Durham scaling [14] for the critical current density was applied and an average strain of -0.8% was assumed in the scaling, again in order to best fit the measured voltage signals. Other assumptions and fitting parameter choices, strictly peculiar of the electromagnetic part of the THELMA model (e.g., contact resistances between cable and jacket, etc.), are discussed in [9], [10].

IV. Results and Analysis

We consider here the $I_{\rm C}$ test at 6.8 K, with 10.78 T background field, run 101005 (a repetition run, 111006, was also performed, giving similar results). The transport current is ramped-up almost linearly @ ~139 A/s up to ~68 kA, then kept constant for a while and finally dumped without quench.

We start presenting the computed results corresponding to measured quantities (e.g., voltage on the jacket, jacket temperatures), in order to gain confidence in the accuracy and reliability of the computed results; then we move to the "predictions" self-consistently included in the same simulation, i.e. the evolution of the current distribution and on the temperature distribution on the cable cross section.

The computed and measured voltage-current characteristics are compared in Fig. 3. Very good agreement is obtained in the case of the V4V10 voltage (albeit partly due to the somewhat ad-hoc choice of the cable n index, see above). In the case of the voltage rings we find a qualitative agreement with a comparable spread of the signals, some overestimation of the V increase at large I (related to the assumption of a single n index for the whole cable) and some disagreement in the initial inductive step, the latter being possibly attributable to the uncertainties in reproducing the cabling scheme of the measuring system. In Figs. 3(c), 3(d) the results of our self-consistent model (including thermal-hydraulics) are also compared to those of a purely electromagnetic model, which assumes the same temperature (= that measured on the jacket) for all cable components on a given cross section [10]. It is seen in the insets that some differences appear between the two computed characteristics in the last phase of the run; this is expected, because the Joule source localized in the strands becomes then increasingly significant.

In Fig. 4 we compare computed jacket temperatures with measured values at the different thermometer locations. All measured temperatures reported here and below have been recalibrated with respect to the raw data, based on the same approach as presented in [12], i.e., with reference to T4, for which the raw data are represented in the figure. Here, however, as opposed to [12] where only the temperature increase in the HFR was relevant, we are also interested in the absolute accuracy of T4 with respect to $T_{\rm in}$, because that is needed for the *joint* calorimetry. This may be roughly assessed by considering the offset of T4 with respect to the measured inlet temperature at 4.5 K (baseline run at zero current [12]) and amounts to ~60 mK, which, in this case, exactly compensates the correction discussed above due to heat transfer in the joint not being accounted by the model. Note also that the thermal-hydraulic model describes the whole jacket as isothermal on the cross

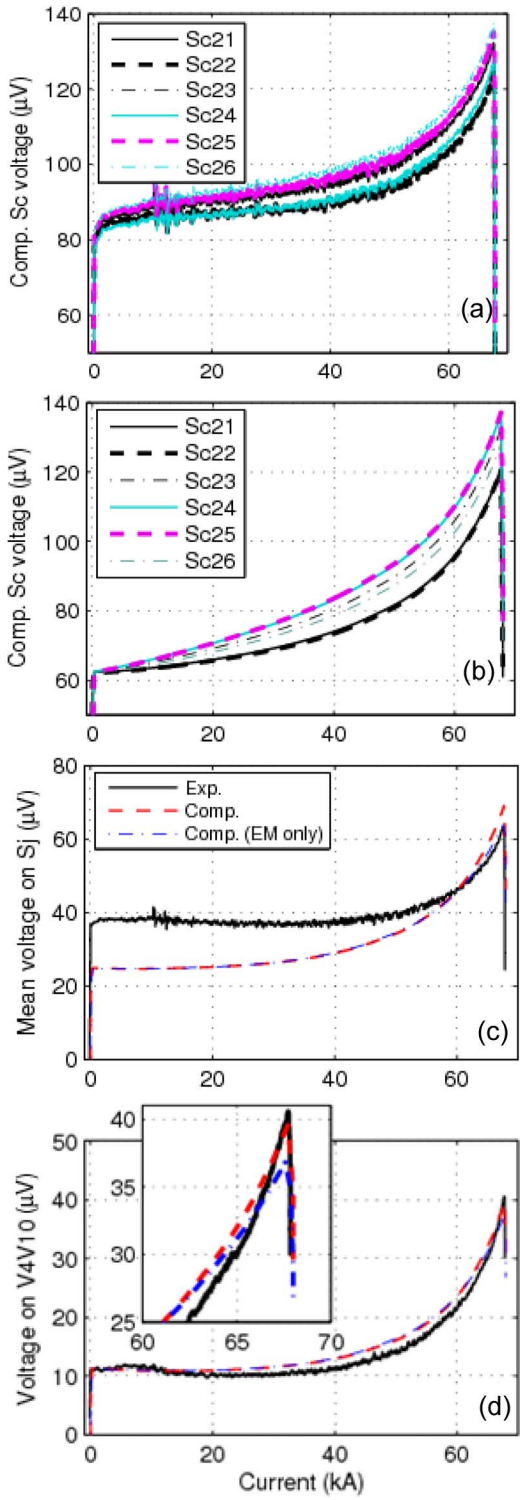

Fig. 3. Computed vs. measured voltage-current characteristics: (a) measured by Sc voltage ring; (b) computed on Sc voltage ring; (c) measured average (solid curve) and computed average (dashed curves, thermal-hydraulic + electromagnetic model, dash-dotted curves, electromagnetic model only) on Sj voltage ring; (d) measured (solid curve) and computed (dashed curves, thermal-hydraulic + electromagnetic model, dash-dotted curves, electroma-gnetic model only) between V4 and V10 voltage taps. Inset shows zoom during last phase of transient.

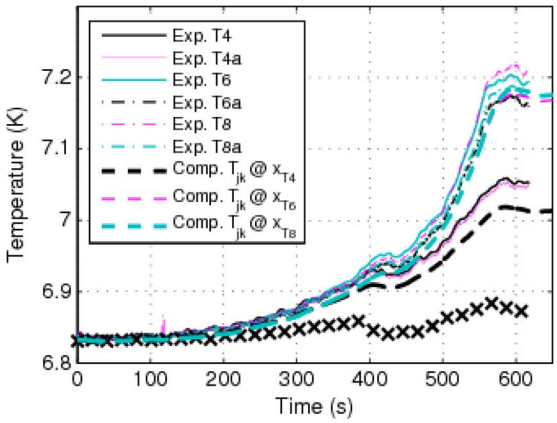

Fig. 4. Computed (bold dashed lines) vs. measured (thin solid and dash-dotted lines) temperature evolution at different locations. Measured inlet helium temperature (crosses).

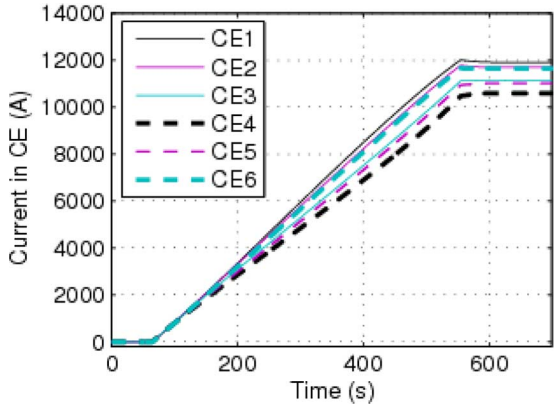

Fig. 5. Computed evolution of the current distribution at the petal level.

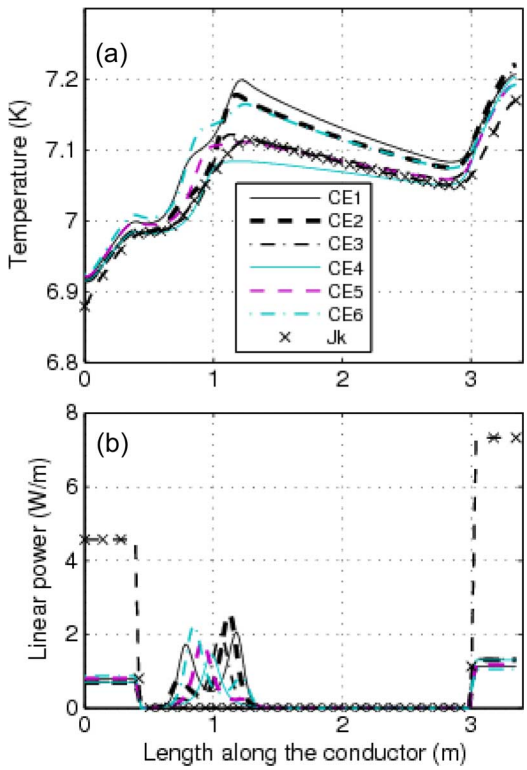

Fig. 6. Computed spatial profiles along the CICC at the end of the current ramp-up ($t = t_{\rm end}$): (a) temperature of the petals (CE1-6) and of the jacket (Jk); (b) corresponding distribution of the Joule power density (W/m) deposited along the CICC in the different CICC components. In the joint and termination regions Jk refers to the power deposited in the Cu saddle.

section, as seen above, so the comparison of this single computed temperature with azimuthally varying measured values is meaningful only in an averaged sense.

The qualitative features of the measured temperature evolution are as follows: from the moment when the current starts to be ramped-up ($t > 50$–100 s), Joule heating in the joint leads to a quadratic increase and departure from $T_{\rm in}$ of the computed temperatures downstream. This ΔT increases until the end of the ramp-up phase ($t = t_{\rm end} \sim 555$–560 s), after which $\mathrm{T4} \sim T_{\rm in} + \Delta T(t_{\rm end})$ with a small transport lag. As soon as a noticeable voltage starts developing ($t > 400$ s), T4 and T6 also start departing from each other, and their difference grows nonlinearly with the VI product. At $t > t_{\rm end}$, the difference between T6 and T4 remains approximately constant. We also note that the spread between temperatures measured at the same axial location increases when going from upstream ($\mathrm{T4} \approx \mathrm{T4a}$ basically anytime) to downstream (e.g., T6 and T6a) of the HFR, thus highlighting a relatively uniform heating of the petals at the joint vs. a somewhat more nonuniform heating in the HFR.

We see that the agreement between computed and measured temperatures in Fig. 4 is reasonable at all axial locations, with typical underestimation of the measured values in the range between 10–20 mK. Although we could look for a further improved agreement at T4, which would then reflect also on the other temperatures downstream, by, e.g., somewhat increasing the resistances at the joint, this would also lead in turn to loss of accuracy elsewhere in the simulation, as the spread of the computed voltages on the rings would increase.

The computed current distribution in the 6 petals evolves accordingly, as shown in Fig. 5. It is seen that the maximum non uniformity at the petal level reaches about 10% as critical conditions are reached at ~400 s (see also below), then decreases to ~5% at the plateau. Moreover, the computed current distribution is uniform in space along the cable (not shown), i.e., current redistribution can occur only at the joint and/or termination [9].

The computed spatial profiles of the 6 petal temperatures and of the jacket temperature at $t = t_{\rm end}$, together with the computed power distribution acting along each of them, are shown in Fig. 6. It is seen that Joule heating in the joint and terminations indeed is almost uniform ($\pm 10\%$). Away from the joint/termination region, the heating power V^*I in the normal zone depends nonlinearly on the total (SULTAN background + return leg background + self) magnetic field, on the temperature and on the current nonuniformity, see Fig. 6(b), and is therefore much more non-uniform, since the twisting petals experience significant field variations. Therefore, in the HFR the resulting temperature gradient computed on the cable cross section is non negligible (~>0.1 K), i.e., much larger than the measured temperature gradients on the jacket, for the above-mentioned values of heat transfer coefficients.

V. Conclusions

The THELMA code has been applied to the coupled thermal-hydraulic/electromagnetic analysis of an I_C test performed in 2007 on the right leg of the TFPRO2 Nb3Sn short sample in the SULTAN facility within the framework of activities for the ITER TF conductors.

The code reproduces fairly well the data measured *outside* the CICC during this test, namely both the voltage-current characteristic and the evolution of the temperature distribution along the sample, although a fraction of the large set of input data needed by THELMA is of difficult independent determination and is used therefore as ad-hoc fitting parameters.

The code predicts at the same time the conditions *inside* the CICC during this test and in particular a relatively small current non-uniformity at the petal level ($\sim<10\%$) which, as such, should not dramatically influence the test interpretation; non-negligible temperature differences ($\sim>0.1$ K) between different petals on the cable cross section in the HFR.

Acknowledgment

RZ and LSR thank CRPP Villigen, Switzerland, for kind hospitality and the CRPP superconductivity group leader, P. Bruzzone, for inviting them to participate in the TFPRO2 tests. We also thank CRPP and F4E for authorizing the use of previously unpublished data.

References

[1] P. Bruzzone, B. Stepanov, R. Wesche, E. Salpietro, A. Vostner, K. Okuno, T. Isono, Y. Takahashi, H. C. Kim, K. Kim, A. K. Shikov, and V. E. Sytnikov, "Results of a new generation of ITER TF conductor samples in SULTAN," *Applied Superconductivity, IEEE Trans.*, vol. 18, no. 2, pp. 459–462, June 2008.

[2] P. Bruzzone, M. Bagnasco, M. Calvi, F. Cau, D. Ciazynski, A. della Corte, A. Di Zenobio, L. Muzzi, A. Nijhuis, E. Salpietro, L. Savoldi Richard, S. Turtu, A. Vostner, R. Wesche, and R. Zanino, "Test results of two European ITER TF conductor samples in SULTAN," *Applied Superconductivity, IEEE Trans.*, vol. 18, no. 2, pp. 1088–1091, June 2008.

[3] M. Ciotti, A. Nijhuis, P. L. Ribani, L. Savoldi Richard, and R. Zanino, "THELMA code electromagnetic model of ITER superconducting cables and application to the ENEA stability experiment," *Supercond. Sci. Technol.*, vol. 19, pp. 987–997, 2006.

[4] M. Breschi and P. L. Ribani, "Electromagnetic modeling of the jacket in cable-in-conduit conductors," *Applied Superconductivity, IEEE Trans.*, vol. 18, no. 1, pp. 18–28, March 2008.

[5] L. Savoldi Richard, M. Bagnasco, and R. Zanino, "Multi-solid multi-channel Mithrandir (M3) code for thermal-hydraulic modelling of ITER cable-in-conduit superconductor," *Fus. Eng. Des.*, vol. 82, pp. 1607–1613, 2007.

[6] R. Zanino, M. Bagnasco, F. Bellina, P. Gislon, P. L. Ribani, and L. Savoldi Richard, "Modeling AC losses in the ITER NbTi poloidal field full size joint sample (PF-FSJS) using the THELMA code," *Fus. Eng. Des.*, vol. 75–79C, pp. 23–27, 2005.

[7] L. Savoldi Richard, P. Bruzzone, N. Mitchell, P. L. Ribani, and R. Zanino, "Assessment of the effect of current non-uniformity on the ITER Nb3Sn good joint short sample DC performance," *IEEE Trans. Appl. Supercond.*, vol. 17, pp. 1382–1385, 2007.

[8] F. Bellina, P. L. Ribani, M. Bagnasco, L. Muzzi, E. Salpietro, L. S. Richard, and R. Zanino, "Analysis and simulation of the ITER-type NbTi bus BarIII with the THELMA code," *IEEE Trans. Appl. Supercond.*, vol. 16, pp. 1798–1802, 2006.

[9] F. Bellina, D. Bessette, M. Breschi, A. Di Zenobio, P. L. Ribani, L. Savoldi Richard, and R. Zanino, Parametric Analysis of the ITER TF Conductor Samples in SULTAN With the THELMA Code this conference.

[10] M. Breschi, P. L. Ribani, and F. Bellina, Voltage-Temperature Characteristics of the ITER TF Conductor Samples this conference.

[11] U. B. Vetrella, A. della Corte, G. De Marzi, A. Di Zenobio, L. Muzzi, L. Reccia, S. Turtu, A. Baldini, P. Bruzzone, E. Salpietro, and A. Vostner, "Manufacturing of the ITER TF full size prototype conductor," *Applied Superconductivity, IEEE Trans.*, vol. 18, no. 2, pp. 1105–1108, June 2008.

[12] L. Savoldi Richard and R. Zanino, "Application of calorimetry to the assessment of ITER Nb_3Sn TF conductor sample performance in SULTAN tests," *Supercond. Sci. Technol.*, vol. 21, p. 105004, 2008, to be published.

[13] L. Bottura, P. Bruzzone, C. Marinucci, and B. Stepanov, "Analysis of transverse heat transfer coefficient in CICC's with central cooling channel," *Cryogenics*, vol. 46, pp. 597–605, 2006.

[14] X. F. Lu, D. M. J. Taylor, and D. P. Hampshire, "Critical current scaling laws for advanced Nb_3Sn superconducting strands for fusion applications with six free parameters," *Supercond. Sci. Technol.*, vol. 21, p. 105016, 2008, to be published.